Subcortical Local Functional Hyperconnectivity in Cannabis Dependence

Supplemental Information

Supplemental Methods

Participants. No experimental activity with any involvement of human subjects took place at the author's institutions. The participants provided written informed consent at Washington University in St. Louis. Extensive demographics and lifestyle/personality data were collected, including the semi-structured assessment for the genetics of alcoholism (SSAGA; see (1) for details).

Cannabis Abuse Cohort. Of the 441 participants, 36 met the DSM-IV criteria for cannabis dependence, which is defined as meeting at least three of the following criteria: 1) development of tolerance; 2) using cannabis in larger amounts or over a longer period than intended; 3) inability to cut down or reduce cannabis use; 4) spending large amounts of time to obtain, use, or recover from the effects of cannabis; 5) giving up important social, occupational, or recreational activities in favor of using cannabis; 6) continued use of cannabis despite its adverse consequences.

Control Cohort. Recent studies have indicated that it is critical in studies of cannabis abuse to select a well-matched control group, particularly on measures of alcohol and tobacco usage (e.g., (2)). Therefore, we took care to find a control group matching on age, sex, education, BMI, anxiety, depression, and alcohol and tobacco usage. To do this, we used the matchControls function in R (library e1071), which calculates a dissimilarity matrix between groups to find the closest match on multiple variables, and critically, can handle numeric, nominal, and ordinal variables in the same model (3). We ran the matchControls function on the 319 subjects who reported using cannabis ≤ 10 times in their life and did not have alcohol dependence to find 32 controls to match the 32 CA participants. This provided a control group that was well-matched on

all variables (p's > .25) except tobacco usage, which was somewhat lower than the CA group (p = .06). Therefore, we stepwise removed the CA participants with the highest tobacco usage and the control participants with the lowest tobacco usage until there was no longer a trend of a difference between groups; this resulted in the removal of two subjects from each group. Thus, the final sample included 30 CA and 30 controls.

Tobacco and Alcohol Usage. We followed the example of a recent study using HCP data (4) to make composite measures of tobacco and alcohol usage. This was done because the SSAGA does not include some measures considered standards in the field, such as "packs per day" for tobacco. Thus, we calculated *Z*-scores across the entire 441-subject population for each measure related to tobacco and alcohol use, and for each participant, we averaged together the *Z*-scores of several measures reflecting past and present substance use. For tobacco, the measures averaged together were: "Total times used/smoked any tobacco in past 7 days", "Cigarettes per day when smoking regularly", "Years since respondent smoked last cigarette", "Years smoked." For alcohol, the measures were: "Total drinks in past 7 days", "Drinks per drinking day in past 12 months", "Frequency of any alcohol use in past 12 months", "Drinks per day in heaviest 12- month period", and "Frequency of any alcohol use, heaviest 12- month period". We reverse-scored measures when appropriate, such that higher *Z*-scores reflect higher levels of substance use.

Cognitive Measures of Interest. For cognition, these included episodic memory (Picture Sequence Memory task), Working Memory (List Sorting Task), Cognitive Flexibility (Dimensional Change Card Sorting Task), Inhibitory Control (Flanker Task), Processing Speed (Pattern Completion Task), Self-Regulation/Impulsivity (Delay Discounting task), Fluid Intelligence (Progressive Matrices), Spatial Orientation (Line Orientation Test), and Verbal Episodic Memory (Word Memory Test).

Volumetric Analysis. For analysis of subcortical volume, we used the output from structural images that had undergone processing in the *PreFreeSurfer* and *FreeSurfer* pipelines. The following steps were implemented: a) gradient distortion correction, b) alignment and averaging of the T1w images from the two sessions, c) brain masking, d) readout distortion correction, e) coregistration of T1w and T2w images, f) bias field correction, and e) nonlinear normalization to MNI space. Subcortical volume output from this pipeline was downloaded in table format from https://db.humanconnectome.org/ for further analysis.

lFCD Voxelwise Regression with Alienation Scores. To identify the region contributing the strongest to the correlation between lFCD and alienation among CA (Fig. 3B), we ran a voxelwise regression using the log-transformed lFCD scores and the z-transformed alienation scores.

Seed-based Functional Connectivity Analysis. To examine whether regions showing group differences in lFCD also exhibit functional connectivity differences with other regions of the brain, we computed seed-based functional connectivity maps using the same methods as our previous work (5, 6). We first "scrubbed" the data using the method proposed by Power and colleagues (7) to remove time points affected by head motions. Briefly, for every time point *t*, we computed the *framewise displacement* given by $FD(t) = |\Delta d_x(t)| + |\Delta d_y(t)| + |\Delta d_z(t)| + r|\alpha(t)| + r|\beta(t)| + r|\gamma(t)|$, where (d_x, d_y, d_z) and (α, β, γ) are the translational and rotational movements, respectively, and *r* (= *50*mm) is a constant that approximates the mean distance between center of MNI space and the cortex and transform rotations into displacements. The second head movement metric was the root mean square variance (DVARS) of the differences in % signal intensity *I*(*t*) between consecutive time points across all voxels, computed as follows: $DVARS(t) = \sqrt{\langle |I(t) - I(t-1)|^2 \rangle}$, where the brackets indicate the mean across brain voxels. We removed

every time point that exceeded the head motion limit $FD(t)>0.5$mm or $DVARS(t)>0.5\%$ via regression.

The fMRI signal time courses were averaged across all voxels for each of the four seed regions showing group differences in lFCD (see clusters in main text, **Figure 2A**). We computed the correlation coefficient between the averaged time course of each seed region and the time course of each voxel in the whole brain for each individual. To assess and compare the resting state correlation maps, we converted the r values, which were not normally distributed, to z scores by Fisher's z transform (8): $z = 0.5\log_e[(1+r)/(1-r)]$.

To further understand if group differences in functional connectivity between specific subcortical nuclei were present, we computed region-to-region functional connectivity analysis of the basal ganglia. Subcortical regions of interest were extracted using a probabilistic atlas generated from high-resolution 7T scans of 30 young adults (9) https://www.nitrc.org/projects/atag; additionally the putamen was extracted from the automated-anatomical labeling (AAL) atlas (10). The average timecourse of each region was correlated with one another, and group differences between CA and controls were assessed with two-sample *t*-tests.

Supplemental Results

Volumetric Analysis. Volumetric data and descriptive statistics are reported in **Supplementary Table S1**.

Power Scaling of lFCD. As we observed previously (11), lFCD values followed a power law distribution, and as such, subcortical lFCD significantly differed from the normal distribution (D'Agostino & Pearson omnibus $K^2 = 8.04$, $p = .018$, **Supplementary Fig. S1A**). To ensure

statistical differences between CA and controls were not due to violation of the assumption of normality, we log-transformed the lFCD values so that the distribution was no longer skewed (D'Agostino & Pearson omnibus K^2 = .47, p = .791, **Supplementary Fig. S1B**). The log-transformed subcortical lFCD remained significantly different between CA and controls, such that CA showed significantly higher subcortical lFCD, $t(58) = 5.88$, $p < 1 \times 10^{-6}$.

lFCD Within-group Results. The results of the subcortical lFCD within each group (one-sample *T*-test) are shown in **Supplementary Fig. S2**.

lFCD Voxelwise Regression with Alienation Scores. At an exploratory threshold of p < .005 uncorrected, one cluster emerged in the general vicinity of the midbrain (maximum at coordinate: x=14, y=-26, z=10; peak t = 5.11; familywise-error cluster-corrected *p*-value = .010; **Supplementary Figure S3**).

Seed-based Functional Connectivity Analysis. In whole-brain functional connectivity analysis using the four clusters from Figure 2A as seed regions, no significant between-group differences emerged at an exploratory threshold of $p < .005$ uncorrected. In region-to-region analysis (**Supplementary Fig. S4**), at an uncorrected p < .05 threshold, the CA group showed higher functional connectivity between left globus pallidus external and left globus pallidus internal, and between the right substantia nigra and left globus pallidus internal (**Supplementary Table S2**). These differences were not significant after correction for multiple comparisons.

Supplementary Table S1. *Freesurfer*-parcellation volumetric estimates for each group. Values are reported as mean ± standard deviation.

	CA	CTRL	*t*-test *p*-value
Whole Brain	1200832 ± 95836	1218402 ± 117078	0.527
Subcortical GM	61727 ± 4359	62250 ± 4442	0.647
Brainstem	22306 ± 2061	22414 ± 2537	0.858
L Thalamus	8477 ± 830	8582 ± 686	0.595
L Caudate	3842 ± 409	3940 ± 552	0.440
L Putamen	5764 ± 529	5819 ± 640	0.719
L Pallidum	1410 ± 198	1395 ± 213	0.784
L Hippocampus	4211 ± 581	4439 ± 335	**0.068**[†]
L Amygdala	1517 ± 206	1576 ± 173	0.234
L Accumbens	589 ± 98	567 ± 83	0.359
R Thalamus	7636 ± 701	7446 ± 532	0.242
R Caudate	3968 ± 446	4065 ± 595	0.475
R Putamen	5694 ± 544	5825 ± 548	0.358
R Pallidum	1541 ± 202	1566 ± 164	0.600
R Hippocampus	4442 ± 425	4488 ± 371	0.654
R Amygdala	1631 ± 176	1658 ± 167	0.536
R Accumbens	608 ± 106	616 ± 89	0.770

NOTE: GM = Gray Matter; L = Left; R = Right

Supplementary Table S2. Significance testing for seed-based connectivity results between regions of interest within the basal ganglia. Values represent the *p*-value of the two-sample *t*-test comparing the CA (n=30) and control (n=30) groups. Subcortical regions of interest were extracted using a probabilistic atlas generated from high-resolution 7T scans of 30 young adults (9) https://www.nitrc.org/projects/atag; additionally the putamen was extracted from the AAL atlas.

	GPe_L	GPe_R	GPi_L	GPi_R	SN_L	SN_R	STN_L	STN_R	put_L
GPe_L									
GPe_R	0.42755								
GPi_L	**0.02255**	0.86512							
GPi_R	0.58503	0.17386	0.95901						
SN_L	0.14753	0.07037	0.42796	0.66545					
SN_R	0.82073	0.79915	**0.03961**	0.99968	0.3638				
STN_L	0.14626	0.3704	0.67026	0.98062	0.73056	0.98668			
STN_R	0.89007	0.93429	0.25268	0.22349	0.76662	0.48872	0.67093		
put_L	0.39048	0.90651	0.82226	0.6967	0.28599	0.81354	0.32484	0.21936	
put_R	0.13277	0.17789	0.09008	0.65034	0.5936	0.06973	0.86313	0.9261	0.32735

NOTE: L=Left, R=Right, GPe=Globus Pallidus External; GPi=Globus Pallidus Internal, SN=Substantia Nigra; STN=Subthalamic Nucleus; put=Putamen.

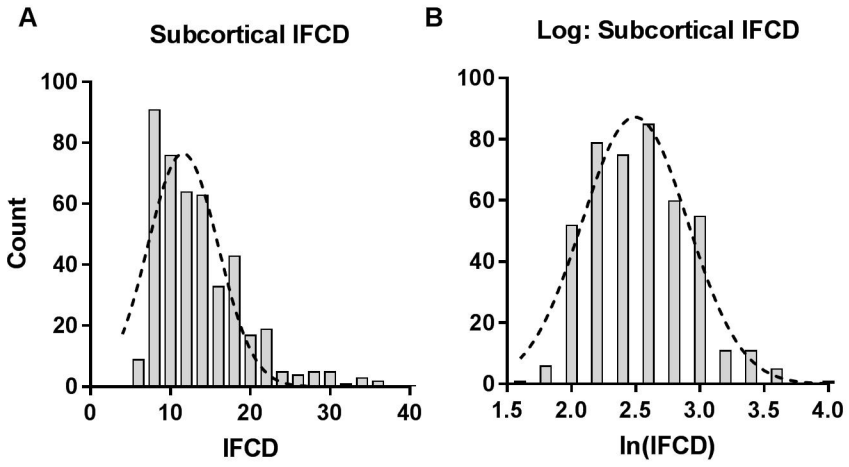

Supplementary Figure S1. Distribution of subcortical lFCD across all 441 HCP subjects. Values represent the average subcortical lFCD of the four regions showing significant differences between CA and controls. A) Raw lFCD values, which showed a significant deviation from the normal distribution (D'Agostino & Pearson omnibus $K^2 = 8.04$, $p = .018$). B) Log-transformed lFCD values, which did not significantly deviate from the normal distribution (D'Agostino & Pearson omnibus $K^2 = .47$, $p = .791$).

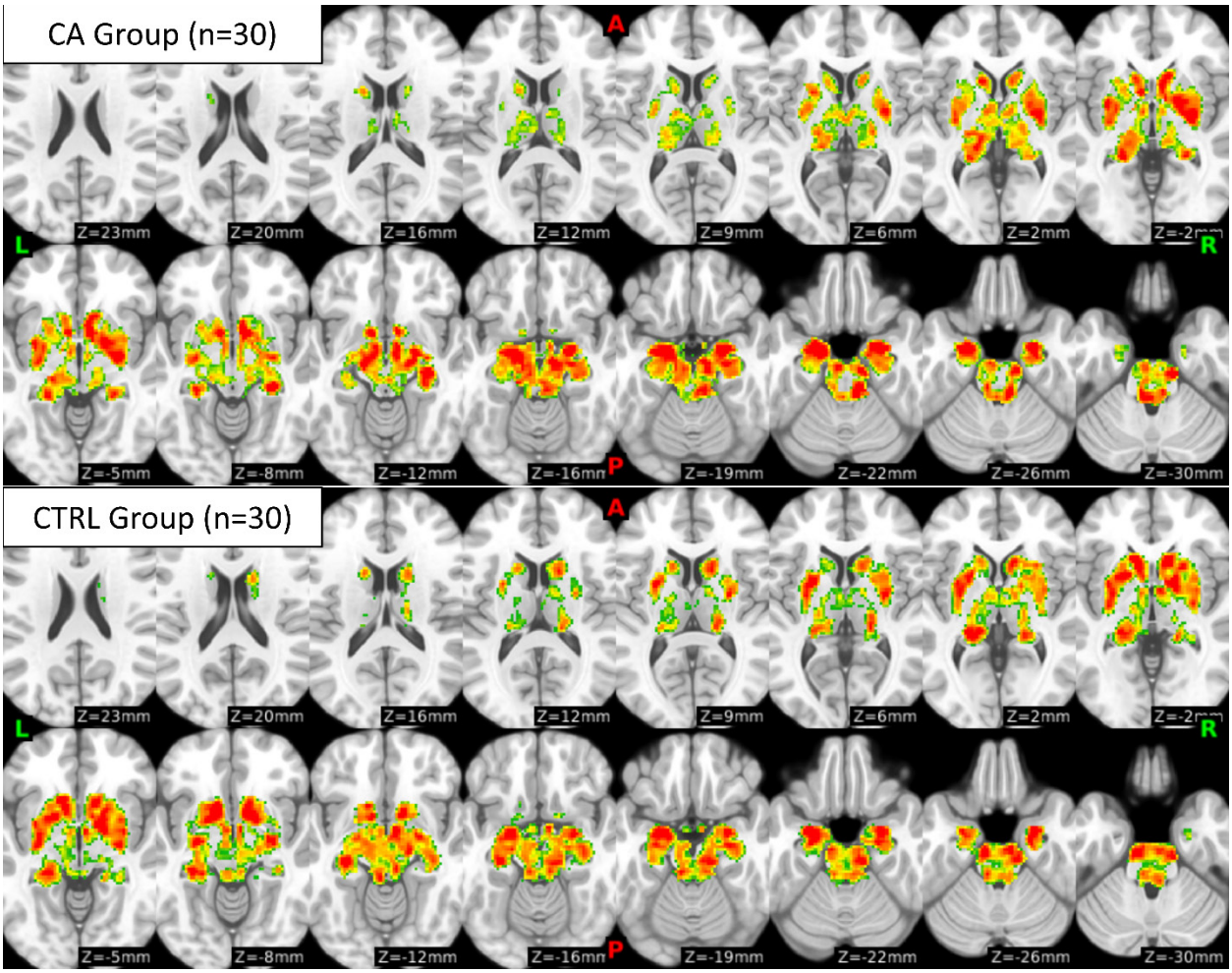

Supplementary Figure S2. One-sample *t*-tests showing subcortical lFCD values separately for the CA group (top two rows) and control group (bottom two rows). Maps are thresholded at $T > 10$, for visualization. Hot colors indicate regions with high local connectivity density.

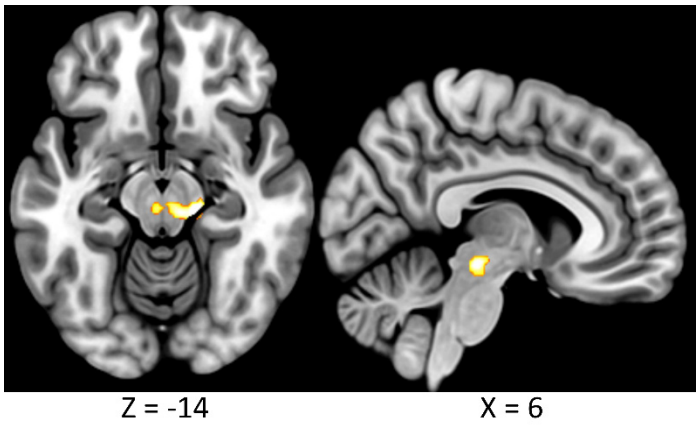

Supplementary Figure S3. Voxelwise regression analysis between log-transformed lFCD scores and the alienation scores among the CA group. Results shown at an exploratory threshold of $p < .005$ uncorrected. One cluster emerged in the vicinity of the midbrain (threshold: $2 < t < 4$).

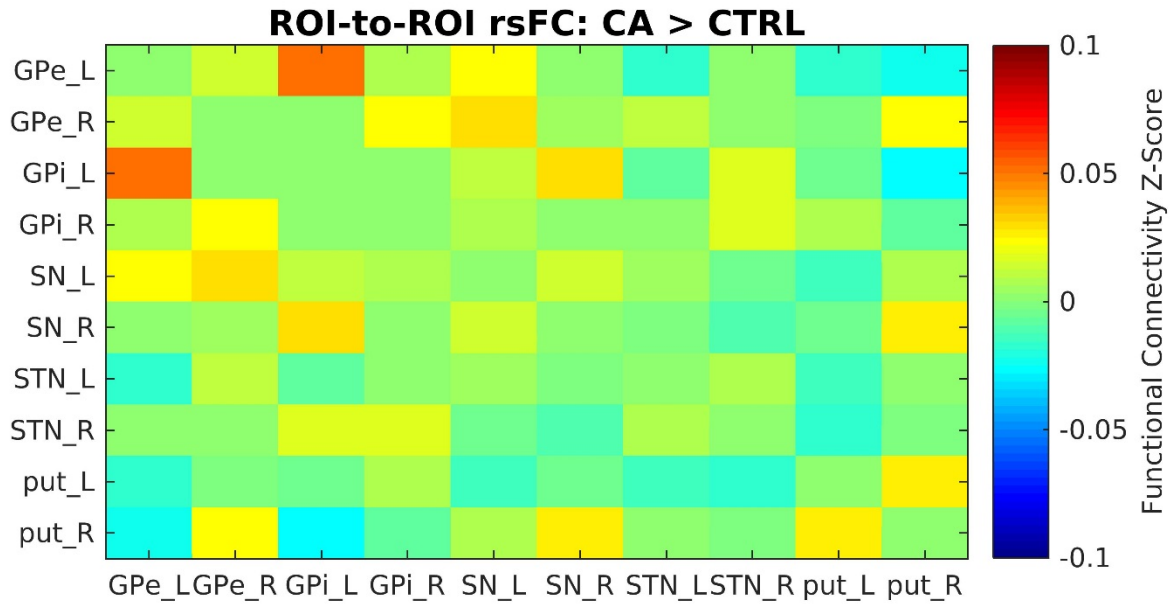

Supplementary Figure S4. Seed-based connectivity results between regions of interest within the basal ganglia. Subcortical regions of interest were extracted using a probabilistic atlas generated from high-resolution 7T scans of 30 young adults (9) https://www.nitrc.org/projects/atag; additionally the putamen was extracted from the AAL atlas (10). Values represent the difference in functional connectivity strength (Fisher's *z*-transformed) between the groups; that is, CA minus control group. Significance testing is reported in Supplementary Table S2. NOTE: ROI=region of interest; L=Left, R=Right, GPe=Globus Pallidus External; GPi=Globus Pallidus Internal, SN=Substantia Nigra; STN=Subthalamic Nucleus; put=Putamen.

Supplemental References

1. Van Essen DC, Ugurbil K, Auerbach E, Barch D, Behrens TEJ, Bucholz R, *et al.* (2012): The Human Connectome Project: A data acquisition perspective. *Neuroimage*. 62: 2222–2231.

2. Weiland BJ, Thayer RE, Depue BE, Sabbineni A, Bryan AD, Hutchison KE (2015): Daily Marijuana Use Is Not Associated with Brain Morphometric Measures in Adolescents or Adults. *J Neurosci* . 35: 1505–1512.

3. Kaufman L, Rousseeuw PJ (1990): *Finding Groups in Data: An Introduction to Cluster Analysis*. *Wiley, New York*. .

4. Orr JM, Paschall CJ, Banich MT (2016): Recreational marijuana use impacts white matter integrity and subcortical (but not cortical) morphometry. *NeuroImage Clin*. 12: 47–56.

5. Manza P, Zhang S, Hu S, Chao HH, Leung H-C, Li C-SR (2015): The effects of age on resting state functional connectivity of the basal ganglia from young to middle adulthood. *Neuroimage*. 107: 311–22.

6. Manza P, Zhang S, Li C-SR, Leung H-C (2016): Resting-state functional connectivity of the striatum in early-stage Parkinson's disease: Cognitive decline and motor symptomatology. *Hum Brain Mapp*. 37: 648–662.

7. Power JD, Barnes K a, Snyder AZ, Schlaggar BL, Petersen SE (2012): Spurious but systematic correlations in functional connectivity MRI networks arise from subject motion. *Neuroimage*. 59: 2142–54.

8. Jenkins GM, Watts DG (1968): *Spectral analysis and its applications*. San Francisco: Holden-Day.

9. Keuken MC, Bazin PL, Crown L, Hootsmans J, Laufer A, Müller-Axt C, *et al.* (2014): Quantifying inter-individual anatomical variability in the subcortex using 7T structural MRI. *Neuroimage*. 94: 40–46.

10. Tzourio-Mazoyer N, Landeau B, Papathanassiou D, Crivello F, Etard O, Delcroix N, *et al.* (2002): Automated anatomical labeling of activations in SPM using a macroscopic anatomical parcellation of the MNI MRI single-subject brain. *Neuroimage*. 15: 273–89.

11. Tomasi D, Volkow ND (2010): Functional connectivity density mapping. *Proc Natl Acad Sci*. 107: 9885–9890.